Received September 2003
Revised January 2004
Accepted February 2004

Effect of drain cover on entrapment of air while draining a cylindrical vessel

Satish K. Ajmani
R&D Division, Tata Steel, Jamshedpur, India, and
Swasti S. Mondal and Sukanta K. Dash
Department of Mechanical Engineering, Indian Institute of Technology, Kharagpur, India

Abstract

Purpose – The objective of the research work is to predict the volume of fluid drained from a cylindrical vessel without entrapping air through the drainpipe, and hence predict the location of the free surface of the liquid in the vessel.

Design/methodology/approach – A two-dimensional axi-symmetric numerical simulation has been made using a finite volume method that employs unstructured grids with cell-wise local refinement and an interface capturing scheme to predict the shape of the free surface of water in a cylindrical vessel, thus simulating the entrapment of air in the drainpipe connected to the vessel.

Findings – A drain cover was placed on top of the drainpipe to delay the entry of air into the drainpipe. It was found that an increase in the diameter of the drain cover increases the amount of liquid to be drained out before the air could enter into the drainpipe. It was found that air enters the drainpipe at a particular height of the liquid in the vessel. However, when an initial rotational velocity was imparted to the liquid, the height of liquid when air enters the drainpipe depends on the initial bath height. As the initial bath height increases, air enters the drainpipe at a progressively higher bath height. But surprisingly when the drain cover is put in place the initial bath height, again, has no effect on the height of the liquid (in the vessel).

Practical implications – The outcome of the present research work has direct implications for steel making. If the drainpipe can be connected to the ladle the way it has been discussed in this paper then more steel can be drained before stopping the drainage in order to avoid air or slag entrapment.

Originality/value – The idea of putting a drain cover, using a larger diameter drainpipe and making the drainpipe connection to the vessel different so as to delay the appearance of air at the drainpipe is a new finding and the idea can be used by steel makers.

Keywords Air, Simulation, Finite volume methods

Paper type Technical paper

Nomenclature

c = volume fraction of the fluid
d = diameter of the drainpipe
g = acceleration due to gravity
H_{cr} = height of the free surface just entering the drainpipe
p = pressure

The last author, SKD, is grateful to Tata Steel for financially supporting this work and he is also grateful to the Alexander von Humboldt Foundation for supporting him with a high end PC and CFD software on which the present computations could be carried out.

International Journal of Numerical Methods for Heat & Fluid Flow
Vol. 15 No. 4, 2005
pp. 394-414

0961-5539
DOI 10.1108/09615530510590632

r = radial coordinate
t = time
v = velocity
z = axial coordinate
ρ = density of the fluid
μ = co-efficient of viscosity
ν = kinematic viscosity
σ = surface tension coefficient

Subscripts
r = radial coordinate
z = axial coordinate
1 = fluid 1 (liquid)
2 = fluid 2 (gas)

Introduction

Drainage of liquid steel from a ladle into the tundish is a critical operation in the steel plant, because, while the liquid is being drained it must be ensured that it does not entrap the slag along with it. Normally, slag remains on the top of the liquid steel because it is lighter compared to the steel. When the liquid is being drained, the free surface of the liquid deforms just above the outlet. The deformation goes on increasing with time and finally, the free surface enters the drainpipe where it subsequently breaks into two parts. When the free surface enters the drainpipe, the liquid on top of the free surface also enters the drainpipe and that finally gets discharged into the tundish, which is not a desirable phenomenon because the liquid sitting on the free surface of steel is slag. In the simulation, the liquid on top of the free surface is air and we are conducting the numerical simulation of the free surface of water to find out when air enters the drainpipe. When the free surface enters the drainpipe, the drainage can be manually stopped so that slag cannot enter the tundish through the drainpipe. Here we look for air entrapment into the drainpipe as the occasion when drainage can be stopped.

The objective is to maximize the drainage without the entrapment of air bubble. So we look for some new design, which can achieve it. Normally, the entrapment of air occurs at the centre of the drainpipe. So it is planned to cover the centre of the drainpipe and allow the liquid to flow from the side towards the drainpipe, so that air entrapment can be delayed. The drain cover arrangement is shown in Figure 1. In the actual case when the ladle is carried to the caster the liquid inherently gets some initial motion. If the drainage starts immediately then the vortex starts quickly which entraps slag and carry that into the outlet of the drainpipe. It is believed that such an arrangement can stop the early appearance of vortex and the quality of casting can be improved due to the absence of slag.

Dubke and Schwerdtfeger (1990) have studied the effect of a stopper rod on the formation of a vortex and an air core in the nozzle (outlet pipe) with cold models using water and mercury as liquids. It was found that in the presence of a stopper rod, the air core develops from below whereas it forms from the surface in the absence of a stopper rod. Surface oscillations were found due to the presence of the stopper rod. In this case, the vortex was found to be detached from the stopper rod and was spinning around it. The frequency of the wave was predicted from the wave theory.

Steffen (1987) carried out model trials from 1:10 to 1:1 scale and plant trials to clarify the influences of the flow phenomena such as "vortex sink" and "drain sink" on slag carryover. Hammerschmid *et al.* (1984) carried out water model study with water and mercury and confirmed that the vortex formation during draining depends strongly on the state of initial rotation in the container. Experiments carried out showed that vortex formation could be suppressed effectively by placing obstacles near the nozzles.

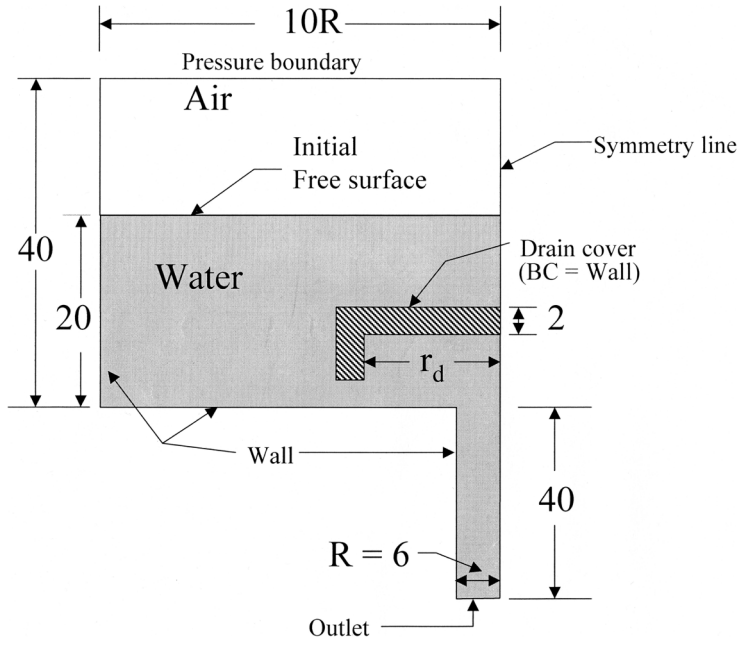

Figure 1.
A schematic view of the draining system of a ladle (all dimensions in mm)

They had used modified outlets, fixed or floating disks and balls over the outlet pipe (where it was connected to the main tank) and have concluded that all these fittings have almost no influence on vortex formation.

Baker (1992) experimented with a number of anti-vortexing devices in ladles to brake up the slag vortexing from the ladle to tundish. But none of the devices produced any encouraging result.

Experiments have been carried out by Sankaranarayanan and Guthrie (1992) to elucidate the parameters that influence the critical limiting height below which a vortexing funnel and draining funnel are formed during ladle teeming operations. They have studied the dependence of vortexing and draining funnel on factors such as vessel and nozzle dimensions, nozzle location, physical properties of the primary liquid and supernatant fluid, residual tangential velocities, etc.

However, the effect of the drain cover and its size on the appearance of the vortex has not been analysed by earlier researchers. So we intend to steer the present work in this direction.

Problem description

Figure 1 shows a cylindrical vessel of radius 60 mm with a drainpipe of radius 6 mm connected to it at the centre. The vessel is initially filled to a height of 20 mm. The drain plug is opened and liquid from the vessel flows out through the drainpipe due to the effect of gravity. The objective is to capture the free surface of the liquid (water for this case) when it just enters the drainpipe. Then it is planned to put drain covers of different radii and see their effect on the free surface and the appearance of the air

bubble at the inlet to the drainpipe. It is also planned to see the effect of initial bath height and initial disturbances of the liquid on the free surface. Initial disturbances (initial flow field) those occur in real life cannot be simulated numerically because no one knows what is the initial velocity field that has been acquired by the fluid due to the disturbances. But it has been seen experimentally that vortex starts quickly if there are initial disturbances in the liquid in the form of initial velocity either small or large. If the initial disturbance is small then vortex starts late compared to a case of higher initial disturbances. So it is thought that the initial disturbances can be simulated by specifying a small angular velocity to the fluid at time $t = 0$, and then start the computation till the free surface enters the drainpipe while the wall is at rest always during the computation. Normally, the initial disturbances that is present in the fluid in terms of its local velocity gets converted to angular velocity and the angular velocity increases towards the centre of the drainpipe causing an early vortex to appear at the centre. It is thought that the drain cover will effectively cut down the transformation of initial velocity to angular motion and will help to delay the appearance of vortex at the drainpipe.

Governing equations

The finite volume method for incompressible viscous flows with free surface is described in detail in Muzaferija and Peric (1999); here we describe it only briefly. The starting point are the conservation equations for mass, momentum, and scalar quantities (e.g. energy or chemical species) in their differential form.

Continuity:

$$\frac{\partial v_{\mathrm{r}}}{\partial r} + \frac{v_{\mathrm{r}}}{r} + \frac{\partial v_{\mathrm{z}}}{\partial z} = 0 \tag{1}$$

Momentum

In radial direction: r

$$\rho\left(\frac{\mathrm{D}v_{\mathrm{r}}}{\mathrm{D}t}\right) = -\frac{\partial p}{\partial r} + \mu\left(\nabla^2 v_{\mathrm{r}} - \frac{v_{\mathrm{r}}}{r^2}\right) + F_\sigma i \tag{2}$$

Axial direction: z

$$\rho\left(\frac{\mathrm{D}v_{\mathrm{z}}}{\mathrm{D}t}\right) = -\rho g - \frac{\partial p}{\partial z} + \mu(\nabla^2 v_{\mathrm{z}}) + F_\sigma k \tag{3}$$

where,

$$\nabla^2 = \frac{\partial^2}{\partial r^2} + \frac{1}{r}\frac{\partial}{\partial r} + \frac{\partial^2}{\partial z^2}, \quad \left(\frac{\mathrm{D}}{\mathrm{D}t}\right) = \frac{\partial}{\partial t} + (U \cdot \nabla)U \text{ and } U = v_{\mathrm{r}} i + v_{\mathrm{z}} k$$

A single momentum equation (equations (2) and (3)) is solved throughout the domain, and the resulting velocity field is shared among the phases. Laminar solution is desired for the present study because the geometrical dimensions are small enough to cut off any turbulence. The momentum equation, shown in equations (2) and (3), is dependent on the volume fractions of all phases through the properties ρ and μ.

Surface tension and interface capturing

Interface-capturing method and HRIC (high-resolution interface capturing) scheme of Muzaferija and Peric (1999) have been used to simulate the free-surface effects. In addition to the conservation equations for mass and momentum, a transport equation for void fraction of the liquid phase c has been introduced:

$$\frac{\partial c}{\partial t} + U \cdot \nabla c = 0 \tag{4}$$

The grid extends to both liquid and gas phase; the void fraction c is set equal to 1 for CVs filled by liquid and 0 for CVs filled by gas. Both fluids are treated as a single effective fluid whose properties vary in space according to the volume fraction of each phase, i.e.

$$\rho = \rho_1 c + \rho_2(1 - c), \quad \mu = \mu_1 c + \mu_2(1 - c) \tag{5}$$

where subscripts 1 and 2 denote the two fluids (e.g. liquid and gas).

The effects of surface tension at the interface between two fluids are taken into account through a body force as a function of the volume fraction c, which is achieved by introducing the *continuum surface force* (CSF) model (Brackbill *et al.*, 1992). The CSF model uses the smoothed field of c to define a unit vector normal to the interface with the help of the gradient vector of c; the divergence of this unit vector defines the curvature of the interface, κ. The surface tension force per unit volume (F in equations (2) and (3)) and the curvature can thus be expressed as:

$$F_\sigma = \sigma \frac{\rho \kappa \nabla c}{\frac{1}{2}(\rho_1 + \rho_2)} \quad \kappa = -\nabla \cdot \left(\frac{\nabla c}{|\nabla c|} \right) \tag{6}$$

where σ is the surface tension coefficient and ρ the volume averaged density computed from equation (5). Equation (6) shows that the surface tension source term for a cell is proportional to the average density in the cell.

Air bubble model

When a bubble is entrapped in the liquid it experiences three kinds of forces on it apart from its own weight. One is the surface tension force at the interface, the second one is the viscous force on the surface as well as everywhere inside the bubble and the third is the surrounding pressure force on it. Due to incorporation of a continuum surface force model as per equations (2) and (3), we take care of the viscous force and the surface tension force acting on any cell at any moment. The pressure gradient force is always present as it is imbedded in the momentum equations (2) and (3). So inherently the momentum equation has all the required components in it to describe the bubble dynamics when we incorporate a continuum surface force model. So separate equations describing bubble physics and its movement is not required as it is already imbedded in equations (2) and (3). The entrapment of a bubble is activated when the surface overturns and intersects itself entrapping the surrounding air into the liquid. No separate activation mechanism is required in the numerical model as the velocity field is computed for a single fluid with varying local properties. If a bubble is present then the cells will have a value of $c = 0$ and the boundary of the bubble will have a value of c lying between 0 and 1 and the physical properties of the local fluid will be computed

according to equation (5) for all those cells having a value of c between 0 and 1. Velocity is computed everywhere and the velocity of the interface is also computed time to time. So the movement of the interface or the bubble can be tracked with time. The present model can therefore describe the entrapment of air bubble in the liquid and its movement in the liquid as well its coalesces or fragmentation. The use of the model to predict the movement of air bubble, its coalescence and fragmentation has been shown in the work of Dash *et al.* (2004).

Boundary conditions

The set of differential equations (1)-(3) have been solved with a set of realistic boundary conditions. The top surface of the cylinder opened to the atmosphere is given a pressure boundary condition where the pressure was set to one atmosphere. The back flow volume fraction of air was set to 1 on this boundary. The outlet was given a zero gradient condition for all the variables except for the velocity components, which were computed from the pressure boundary condition of zero pressure. The back flow volume fraction for air was also kept to be 1 on this boundary. At the symmetry plane, zero gradient conditions in a direction normal to the symmetry plane for all the variables were used. At the wall zero gradient condition for the volume fraction, c has been used because the quantity c, cannot diffuse into the wall. With all these set of boundary conditions one initial condition for all the variables are needed to start the solution.

Initial condition

At time $t = 0$, all velocity components were set to 0. But for the case of rotating cylinder the fluid was set to $u = -\omega r \sin\theta$, $v = \omega r \cos\theta$ everywhere, while the walls were kept at zero velocity. The volume fraction, c, was set to zero in the air and set to 1 in water. For the steel slag and air case, appropriate volume fraction was set to describe the initial location of all the three fluids while steel was described to be the primary fluid for which the volume fraction equation was not solved (because volume fraction of air and slag will predict the volume fraction of steel at any point).

Properties of the fluids used in the simulation

The physical properties of the fluids used in the numerical simulation are given in Table I.

Numerical solution methodology

The solution domain is subdivided into a finite number of non-overlapping control volumes (CVs); in the centre of each CV lies the computational point at which the known quantities are specified and the unknown variables are to be computed. Local refinement was used to achieve finer resolution in regions of rapid change of the

Property	Water	Steel	Slag	Air
ρ (kg/m^3)	988.3	7100 1.28 (air-steel)	–	1.225
σ (N/m)	0.073 (air-water)	1.11 (slag–steel)	0.25 (air-slag)	–
μ (Pa S)	0.001013	0.006482	0.129	1.8×10^{-5}

Table I.

variables, as shown in Figure 2. The CVs are treated as polyhedra and can have an arbitrary number of neighbours (unstructured grids).

Equations (1)-(3) are applied to each CV and then discretised, leading to one algebraic equation per CV in which variables from immediate neighbours also feature. All integrals are approximated using midpoint rule, i.e. the function to be integrated is evaluated at the centre of the integration domain and multiplied by the area, volume or

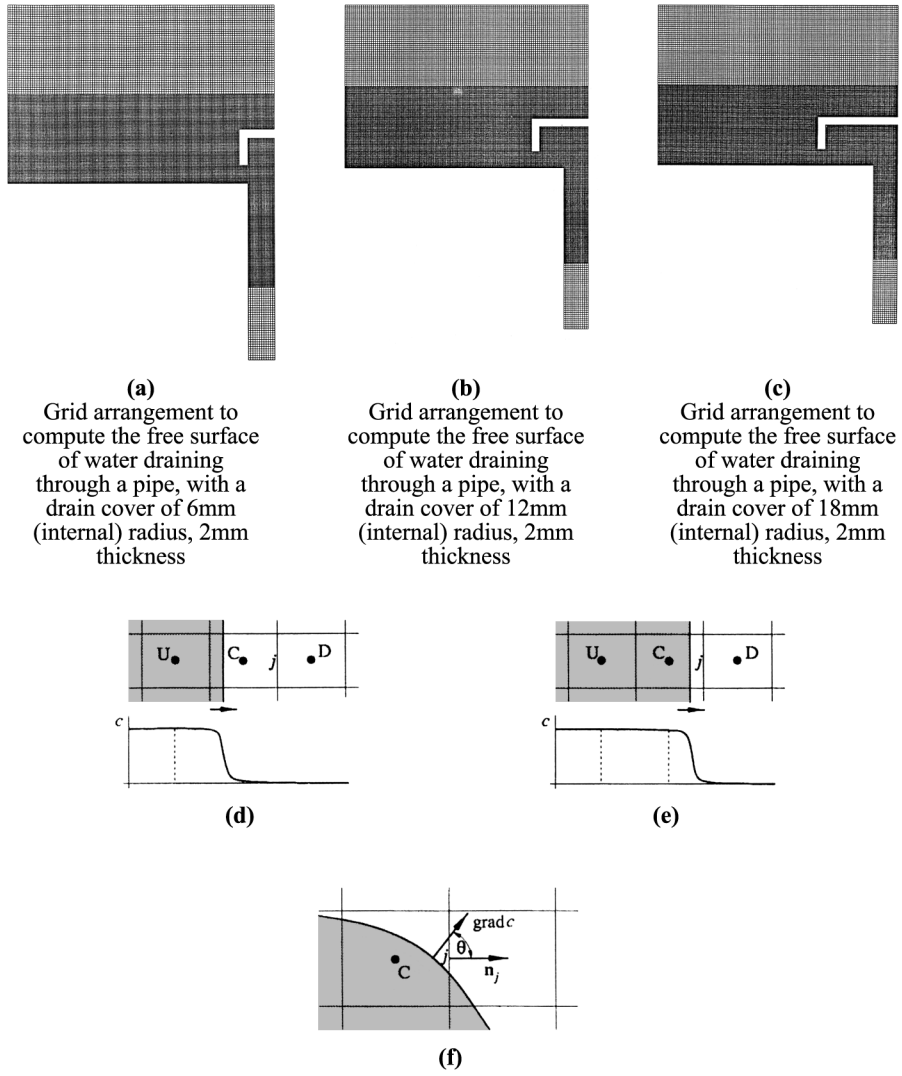

Notes (d, e, f only): On the computation of cell face fraction at face j – Shaded portion represents presence of c, U = up stream, C = center node where c is being computed, D = down stream node

Figure 2.

time interval over which the integration takes place. In order to evaluate the function at the centre of the integration domain, one needs to introduce further approximations: interpolation and differentiation. In space, linear interpolation is used, while in time either linear or quadratic shape functions are used. The diffusive fluxes require that the derivatives in the direction normal to CV faces be computed at each cell-face centre; these are obtained from linear shape functions with the help of least-squares method or Gauss-theorem. The integration in time is fully implicit (first-order Euler implicit method). The spatial integration is also of either first- or second-order, depending on the approximation of convected variable in convective fluxes (upwind or central differencing, or a blend of the two). In the present computation, first-order upwinding scheme was adopted for the convective fluxes with a blending factor of 0.5. In order to keep the computational molecule limited to cell centre node and centres of nearest neighbour cells, *deferred-correction* approach is used: low-order approximations which use only nearest neighbours are used to construct the coefficient matrix, and the difference between the desired approximation and the low-order one is computed explicitly from the values obtained in the previous iteration and added to the source term on the right-hand side of the equation. More details on individual steps in the discretisation procedure can be found in Muzaferija and Peric (1999).

In order to calculate the pressure field and to couple it properly to the velocity field, a pressure-correction method of SIMPLE-type (Patankar and Spalding, 1972) is used. Velocities computed from momentum equations using pressure from previous iteration step are corrected to enforce mass conservation, and the correction to cell-face velocity is proportional to the gradient of pressure correction, leading to a Poisson-type pressure-correction equation. When solving the equation (4), a special interpolation method is used to compute the cell-face value of the volume fraction c (HRIC-scheme; Muzaferija and Peric, 1999), which is designed to keep the interface sharp (i.e. avoid spreading due to numerical diffusion) and to maintain c bounded (i.e. c is not allowed to become less than zero or greater than unity). This is achieved by blending the upwind and downwind approximations, with blending factor being a function of the local profile of c, the orientation of interface relative to cell face, and the local Courant number. The following equations show how the cell-face value of volume fraction c is computed at the cell face j according to the HRIC scheme

$$c_j = c^{**}_j(c_{\mathrm{D}} - c_{\mathrm{U}}) + c_{\mathrm{U}}$$

where

$$c^{**}_j = c^{*}_j\sqrt{\cos(\theta)} + c_C\left(1 - \sqrt{\cos(\theta)}\right)$$

and θ represents the angle between the normal to the interface (found out by the gradient vector of c) and the normal to cell face (see Figure 2(d)-(f)).

$$c^{*}_j = \begin{cases} \bar{c}_j & \text{if } \mathrm{Co} < 0 \\ c_{\mathrm{C}} + (\bar{c}_j - c_{\mathrm{C}})\frac{0.7-\mathrm{Co}}{0.7-0.3} & \text{if } 0.3 \le \mathrm{Co} < 0.7 \\ c_{\mathrm{C}} & \text{if } 0.7 \le \mathrm{Co} \end{cases}$$

where the local Courant number is $\mathrm{Co} = (v \cdot nS_j\delta t/\delta V_c)$ (S_j is the surface area at j and δV_{C} is the volume of the cell C.

$$\bar{c}_j = \begin{cases} c_C & \text{if } c_C < 0 \\ 2c_C & \text{if } 0 \le c_C \le 0.5 \\ 1 & \text{if } 0.5 \le c_C \le 0.5 \\ c_C & \text{if } 1 \le c_C \end{cases}$$

More details on the method are available in Muzaferija and Peric (1999). It is implemented in the commercial code Comet[1], which has been used in this study.

Time step used for the integration of the equation was 0.00005 s at the start of the solution and later on it was slowly increased to 0.0001 s and then decreased to 0.00002 s when the free surface was about to enter the drainpipe. About 2-3 iterations per time step was required for a converged solution to be achieved at each time step. The cells at the drainpipe had a maximum size of 0.25 mm × 0.25 mm (Figure 2(a)-(c)), which could capture the interface very sharp. Cell sizes near the outlet of the drainpipe were 0.5 mm × 0.75 mm. Finer cells are not required at the outlet because the free surface is not expected to reach there. Cells inside the cylinder are having the same size (0.25 mm × 0.25 mm) like that of the cells present at the inlet of the drainpipe. But the cells present above 20 mm level (measured from the bottom of the cylinder) are kept to be larger (0.5 mm × 0.5 mm) because the free surface is also not expected to be present in that zone (the zone consists of air and when the free surface recedes away, air immediately fills up the vacant zone). Grid-independency test for the present computation was done by making the cell size half everywhere in the computational domain. It was found that there was practically no difference in the location of the free surface compared with the present cell size for which results are reported here.

Results and discussions

Figure 2 shows the grid arrangement in the computational domain along with the drain covers of different radii. Initially, water was kept to a level of 20 mm. So the grids are made finer up to this level so that the free surface can be captured very sharp. In the drainpipe also, grids are made finer so that the entry of the free surface into it can be captured well. In the locally refined area, the minimum cell size is 0.25 mm. It must be marked that the cells are coarser in the upper part of the vessel. Air remains in the upper part of the vessel and there will be no significant velocity change in that zone, so finer grids are not required there. As our objective is to capture the free surface when it just enters the drainpipe and then stop the computation, so there is no need to put finer grids towards the outlet of the drainpipe also.

Effect of radius of the drain cover

A simulation is done without the drain cover and that is shown in Figure 3(a). It can be seen from Figure 3(a) that the free surface comes to a height of 9.3 mm near the outer wall (the millimetre scale can be read near the outer wall) when it has just entered into the drainpipe. If the draining continues beyond this point then air will be drained out along with water. From casting point of view such a situation is not desirable and hence draining has to be stopped at this point in order to keep the metal quality high otherwise it will be spoiled by the slag entrapment. So when the free surface of water just enters the drainpipe we stop the computation and evaluate how much of liquid has

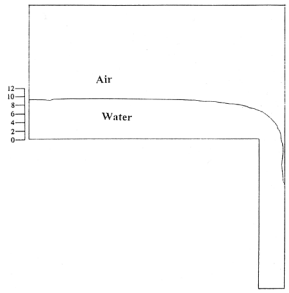

(a)
Free surface of water just entering the drainpipe inlet showing the entry of outside air into it

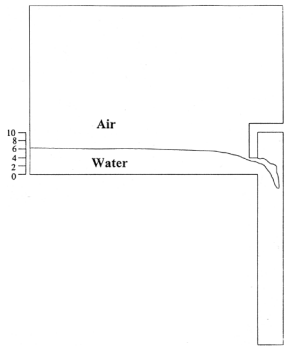

(b)
Free surface of water just entering the drainpipe inlet while flowing under a drain cover of 6mm radius (air is just entering into the pipe)

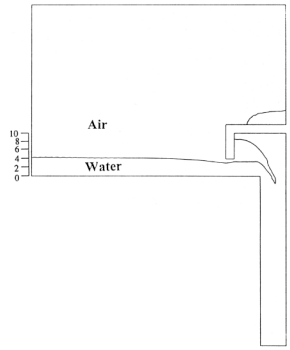

(c)
Free surface of water just entering the drainpipe inlet while flowing under a drain cover of 12mm radius (air is just entering into the pipe)

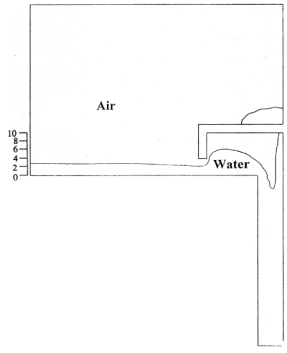

(d)
Free surface of water just touching the drainpipe inlet while flowing under a drain cover of 18mm radius (air is just entering into the pipe)

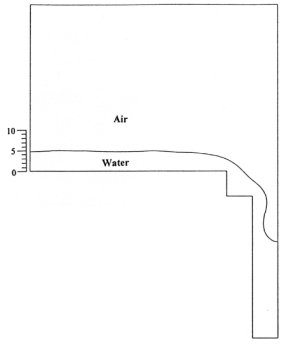

(e)
Free surface of water just entering the inlet of the drainpipe (Drainpipe connected to the vessel through another pipe, which has a radius of 12mm and height of 6mm)

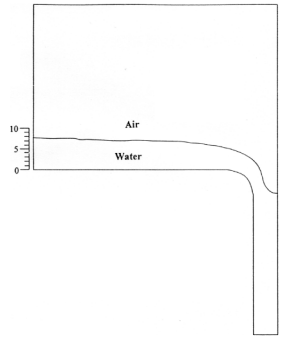

(f)
Free surface of water just entering the inlet of the drainpipe (Drainpipe connected to the vessel through another Frustum shaped pipe which has a larger radius of 12mm, smaller radius of 6mm and height of 6mm)

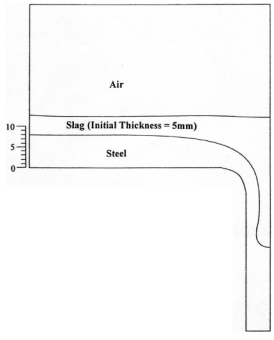

(g)
Free surface of liquid steel and slag just entering the inlet of the drainpipe, (Drainpipe connected to the vessel through another Frustum shaped pipe, having a larger radius of 12mm, and small radius of 6mm and a height of 6mm)

Figure 3.

been drained out (volume of fluid drained out in each case is shown in Table I). It is also the objective that the draining should be as high as possible without the entrapment of air.

In Figure 3(b), a drain cover of radius 6 mm is put at a height of 10 mm from the bottom of the vessel. There is 4 mm gap at the outer edge of the drain cover through which the fluid can come into the drainpipe for its drainage. It can be seen that the free surface has come down to a level of 6 mm before its entry into the drainpipe. So when a comparison is made between the case of no-drain cover and drain cover, it can be concluded that with a drain cover it is possible to drain out more liquid without entrapping air into it. It can also be seen from Figure 3(c) and (d) that as the radius of the drain cover increases, more and more liquid can be drained out of the vessel without the entrapment of air. When the radius of the drain cover is 12 mm, the free surface remains at a height of 4.1 mm before its entry into the drainpipe and when the drain cover radius is 18 mm, the free surface level falls to 2.5 mm after which it can enter the drainpipe.

When there is no drain cover, the fluid gets a straight path into the drainpipe for its drainage. Near the drainpipe inlet, the velocity of the fluid increases causing the radial pressure drop to increase. The dimple formed on the free surface grows in size and finally, the free surface enters the drainpipe causing air to be entrapped in the liquid, which is being drained out. When there is a drain cover, the fluid cannot enter the drainpipe vertically down, but it has to come from the side of the drain cover into the drainpipe. This helps the free surface to arrive late at the drainpipe causing more of liquid to be drained out and thus the free surface comes to a lower height before it could enter the drainpipe. As the radius of the drain cover increases, the liquid has to enter the drain cover from a far off distance, so also the air moving on top of the liquid. But the air rises up inside the drain cover, which causes the liquid to swell inside the drain cover. This swelling effect of the liquid delays the entry of air into the drainpipe. The swelling of the liquid or of the free surface can be seen very clearly in Figure 3(d) where the drain cover radius is 18 mm. When the drain cover is small in size, the swelling of free surface does not take place at all. The free surface simply comes into the drainpipe without swelling any further.

Different arrangement of drainpipe connection

In Figure 3(e) and (f), two new types of drainpipe connections are shown compared to the cases shown in Figure 3(a)-(d) where the drainpipe is connected to the vessel without any attachment. In Figure 3(e) the drainpipe is connected to another pipe having a diameter of 24 mm and a height of 6 mm. All other dimensions remain exactly the same as in Figure 3(a)-(d) or in Figure 1. In Figure 3(f), the drainpipe is connected to a frustum shaped pipe having a base diameter of 24 mm (which is connected to the vessel bottom), top diameter of 12 mm and a height of 6 mm (radius of curvature for the curve side wall is 6 mm). It can be seen from Figure 3(e) and (f) that these types of connections are able to draw more fluid before air could enter into the drainpipe. The geometry in Figure 3(e) can draw as much fluid as the case of a drain cover having a radius of 12 mm. Whereas, the geometry of Figure 3(f) can draw less fluid compared to the geometry of Figure 3(e). However, the geometry of Figure 3(f) draws more fluid compared to the case when the drainpipe was straight connected to the vessel as shown in Figure 3(a). So such types of drainpipe connections can also help to draw more fluid

without entrapping air into it and more study on the parametric aspects of the drainpipe connections can be a scope of the future work.

Drainage of steel in presence of slag and air

Figure 3(g) shows the drainage of steel when there is a top slag layer of 5 mm and the rest of the domain is filled with air. The initial height of liquid steel is kept to be 20 mm and the geometry is exactly kept to be the same like that of Figure 3(f) (although the geometrical dimensions are too small compared to the real life situation for steel drainage, but a comparison of the numerical simulation for this geometry can be meaningful with a water and air system). It should be noted here that a numerical computation for steel drainage in a real life situation, taking the real geometry of the vessel into account can be highly time consuming and may be in some cases not possible if particularly a three-dimensional solution is desired. So if one is interested to compute the height of the free surface at the wall or the amount of steel that has been drained before slag entrapment then he has to start the computation just prior to slag entrapment so that the computational time can be kept realistic. However, such a computation would need the velocity field and the volume fraction field prior to the start of the computation and this is almost impossible to be provided. The only way to simulate such a situation is to make to a scaled down model of the real life situation and perform a computation for that (and later on develop empirical relations from numerical study) which has been attempted in the present work. It should also be noted here that due to the small geometrical dimensions considered here the effect of turbulence has been cut off. If one considers a large geometry then he has to take the effect of turbulence into account and the time of computation would be much higher. From the experiment it has been found out (Sankaranarayanan and Guthrie, 1992) that the height of the draining vortex does not depend on the diameter of the vessel rather on the diameter of the drainpipe. So it is a good idea to take a small vessel and do the experiment for the small set up and compare that with a numerical computation.

The initial volume of water in Figure 3(f) and the initial volume of steel in Figure 3(g) are exactly the same. The amount of water drained before air entrapment is 146.9 cm^3 (Figure 3(f)) where as the amount of steel drained before slag entrapment is 140.2 cm^3 (Figure 3(g)) (the difference in the volume drained is due to the fact that slag has taken out some volume from the drainpipe, if one desires to have exactly the same liquid steel to be drained like Figure 3(f) then he has to allow the free surface to go little more into the drainpipe). The height of the free surface at the wall for both these cases is exactly the same (7.8 mm), which corroborates the fact that water can be used in place of steel and a scaled model can be used to predict the drainage phenomenon. The presence of slag on the top of steel does not influence the drainage of steel very much as because the shape of the free surface in both the cases look almost alike. So a numerical simulation made with water and air may not take the presence of any slag layer into account yet it can predict the drainage of steel almost accurately including its shape of the free surface.

Comparison with experiment

Experiments have been done to find out the height of the free surface at the wall when the free surface at the centre enters the drainpipe. We took exactly the same shape of the cylinder with a drainpipe attached to it at the centre (exactly like Figure 1) and

placed the drain cover of different radii such as 6, 12 and 18 mm just above the drainpipe. Water was filled up to a height of 20 mm and the set up was allowed to settle down for about 5-6 h before the drain plug was opened. Pictures were taken continuously while the draining was going on, so a picture could be obtained just at the point when the free surface entered the drainpipe. Such a picture is shown in Figure 4(a) with no drain cover, which shows the height of the free surface at the wall to be 9 mm (as can be read from the millimetre scale attached with the figure). Figure 4(b) and (c) shows the height of the free surface at the wall when the drain covers of radii 6 and 12 mm are placed over the drainpipe, respectively. An experimental snap shot with a drain cover of 18 mm radius could not be taken very clearly as the height of the free surface was extremely low (about 2.5 mm), so such a picture could not be shown here for comparison. The drained volume of the fluid prior to air to entrapment was also measured and that is shown in Table II. Table II shows a comparison between the

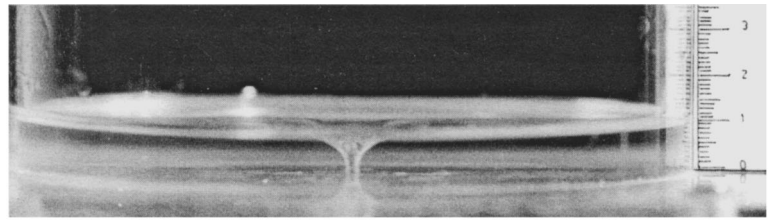

(a)
Experimental snap shot showing the free surface of water in the cylinder when air just enters the drainpipe

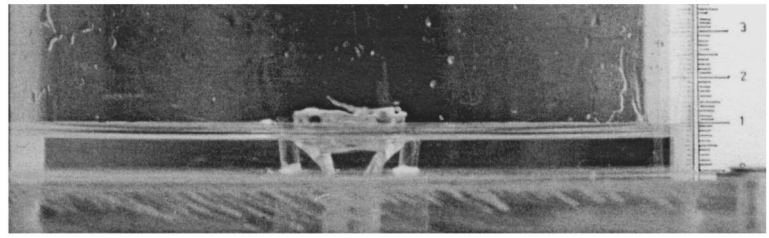

(b)
Experimental snap shot showing the free surface of water, when air just enters the drainpipe under a drain cover having a radius of 6mm

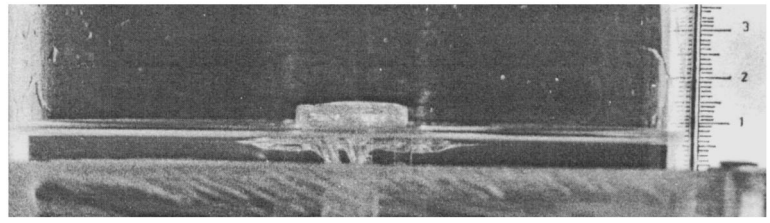

(c)
Experimental snap shot showing the free surface of water, when air just enters the drainpipe under a drain cover having a radius of 12mm

Figure 4.

Case no.	Volume of fluid drained (cc) Computation	Experiment	Height of free surface at the wall (mm) Computation	Experiment
Figure 3(a) (no drain cover)	123.2	125	9.3 (9.2 mm from equation (7))	9.0
Figure 3(b) (drain cover radius = 6 mm)	158.5	150	6	7.0
Figure 3(c) (drain cover radius = 12 mm)	178.7	170	4.1	5.0
Figure 3(d) (drain cover radius = 18 mm)	195.1	190	2.5	2.8
Figure 3(e) (no drain cover, stepped drain pipe)	176	–	4.67	–
Figure 3(f) (no drain cover, frustum shaped drain pipe)	146.9	–	7.8	–

Table II. Volume of fluid drained and height of free surface at the wall when the free surface enters the drainpipe: a comparison between computation and experiment

computation and the experimentally obtained height for the free surface at the wall along with the volume of water drained when the free surface just enters the drainpipe with and without the drain cover.

Use of empirical relation

In literature there are not any empirical relations available to correlate the height of the free surface when that enters the drainpipe with drain cover and with initial angular velocity. However, one relation developed by Harleman *et al.* (1959) to predict the height of the free surface when it enters the drainpipe (without the drain cover and without initial angular velocity being imparted to the fluid) can be used to have a comparison with the present computation

$$\frac{Q^2}{\left[g\left(1-\frac{\rho_2}{\rho_1}\right)H_{cr}^5\right]} = 6.32K^2 \tag{7}$$

where $Q = C_d(\pi d^2/4)\sqrt{2gH_{cr}}$, and K was determined experimentally to be 0.64 by Harleman *et al.* Taking a value of C_d to be 0.85, $d = 12$ mm for the present computation, one can get the height of the free surface H_{cr} to be 9.2 mm from the empirical equation (7) as compared to the computed value of 9.3 mm from the present computation. It can be seen from equation (7) that H_{cr} does not depend on the initial height of the fluid in the vessel and also on the diameter of the vessel. So numerical simulations can take smaller vessel size to predict the height of the free surface before it enters the drainpipe thereby saving on the computational time.

Effect of initial angular velocity

The liquid was filled up to an initial height of 20 mm for all the cases and an initial angular velocity of 0.5 rad/s was imparted to the fluid, but not to the wall. The wall was kept stationary always during the computation. The initial velocity is a sort of acquired disturbance that the fluid has retained in it just before its drainage. Then the computation was started with this initial condition. It can be seen from Figure 5(a) that

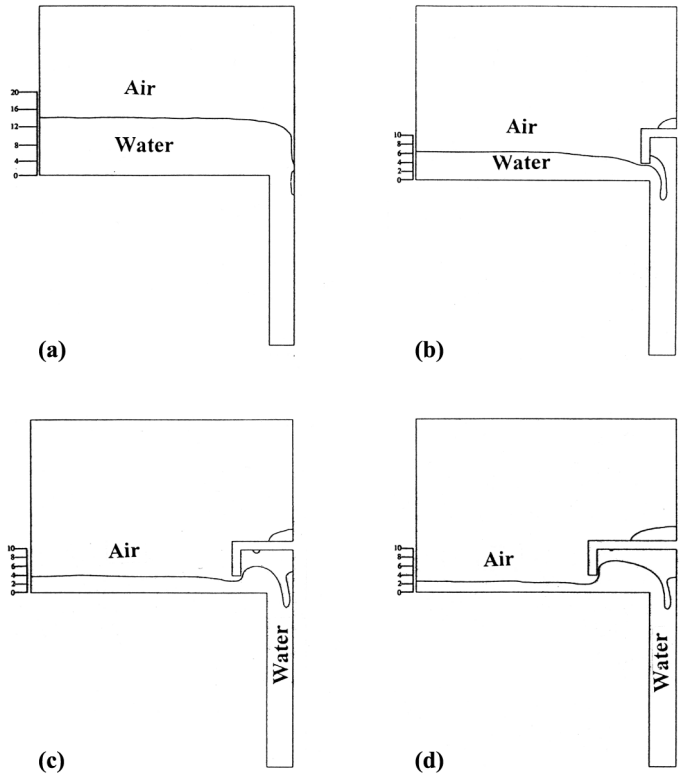

Figure 5.
Effect of initial angular velocity (0.5 rad/s) on the free surface of water entering the drainpipe under a drain cover of radius: (a) 0 mm; (b) 6 mm; (c) 12 mm; and (d) 18 mm

the free surface entered the drainpipe when it is at a height of 14.4 mm near the outer wall. A comparison with the previous case (no initial angular velocity) shows that the free surface has entered the drainpipe much early in the presence of an initial angular velocity of 0.5 rad/s which is considered to be very low.

Figure 5(b)-(d) show the effect of the radius of the drain cover on the free surface. It can be seen that as the radius of the drain cover increases, the height of the free surface near the outer wall decreases before the free surface could enter the drainpipe. Hence, with the presence of the drain cover it is possible to draw more fluid without entrapping air into it. It should be marked from Table III that with the drain cover in place and with initial angular velocity being imparted to the fluid, it is possible to draw almost the same amount of liquid (without entrapping air into it) compared to the case having no initial angular velocity being imparted to the fluid. So the initial disturbances in the form of an initial angular velocity are cut off very effectively due to the presence of the drain cover.

From Table III, a comparison of the height of the free surface near the vessel wall can be read when the free surface is just entering the drainpipe with and without the presence of initial angular velocity. Without the drain cover, the free surface enters the drainpipe much early with the presence of initial angular velocity. But in the presence of a drain cover and initial angular velocity, the free surface enters the drainpipe at a marginally higher height compared to a case of no initial angular velocity only for the case with a

Case no.	Volume of fluid drained (cc)			Height of free surface at the vessel wall (mm)		
	$\omega = 0$ rad/s	$\omega = 0.5$ rad/s	$\omega = 1.0$ rad/s	$\omega = 0$ rad/s	$\omega = 0.5$ rad/s	$\omega = 1.0$ rad/s
Figure 5(a) (no drain cover)	123.2	56.6	54.85	9.3	14.4	15.8
Figure 5(b) (drain cover radius = 6 mm)	158.5	153.8	141.4	6	6.3	8.0
Figure 5(c) (drain cover radius = 12 mm)	178.7	182.0	182.0	4.1	4.0	4.0
Figure 5(d) (drain cover radius = 18 mm)	195.1	190.2	193.0	2.5	2.5	2.3

Table III.
A comparison of the height of the free surface near the vessel wall and the volume of fluid drained before the free surface enters the drainpipe with and without initial angular velocity

drain cover of 6 mm radius. But when the drain cover radius increases the height of the free surface at the vessel wall decreases, with the increase of the initial angular velocity (for the case of 12 mm drain cover) just when the free surface is entering into the drainpipe. For the drain cover of 18 mm radius, the free surface at the wall remains constant with an initial ω of 0.5 rad/s, but when the initial ω is increased to 1 rad/s, the height of the free surface at the vessel wall again marginally falls to a height of 2.3 mm.

Thus, the drain cover has effectively cut down the effect of the initial angular velocity on the arrival of the free surface at the inlet of the drainpipe. Thus, it can be presumed that any disturbance that has been acquired by the fluid in the vessel during its transportation can be effectively cut down by a drain cover and the influence of the disturbances on the amount of liquid to be drained without the entrapment of air can be very much negligible in the presence of a drain cover.

It should be marked from Figure 5(c) and (d) that the free surface swells inside the drain cover before it enters the drainpipe. Under a drain cover of radius 12 mm and without the presence of initial angular velocity there was almost no swelling of the free surface (see Figure 3(c)), but in the presence of initial angular velocity the free surface has swollen considerably under the drain cover (see Figure 5(c)). It can be marked from Figure 6(c) and (d) that the swelling of the free surface under the drain cover (of 12 and 18 mm radius) is considerably high compared to a case of lower initial angular velocity

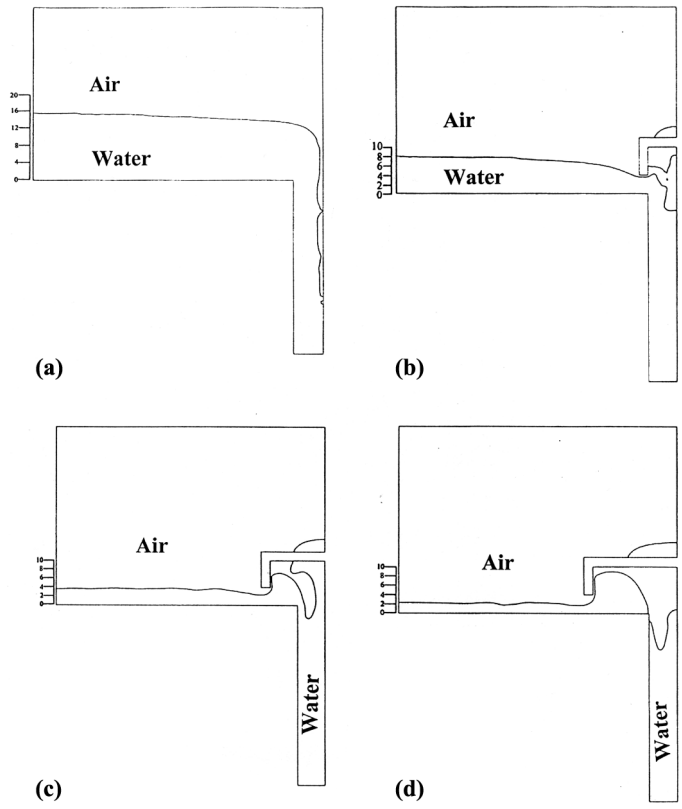

Figure 6.
Free surface of water just entering the drainpipe, initial $\omega = 1.0$ rad/s, drain cover radius for: (a) 0 mm; (b) 6 mm; (c) 12 mm; and (d) 18 mm

(Figure 5(c) and (d)). Due to this swelling effect, the arrival of the free surface at the drainpipe is delayed and more liquid by that time has been drained out causing the level of the free surface at the vessel wall to fall compared to a case of low initial angular velocity where the swelling is low under the drain cover.

Effect of initial bath height

Without initial angular velocity. The vessel was filled up to a particular height at the beginning (20 mm) and the computation was carried on for the drainage. The computation was stopped when the free surface of water just entered into the drainpipe. To see the effect of initial bath height on the free surface of water when it just enters the drainpipe, another set of computations were carried out at a higher initial bath height (40 mm) for all the cases of drain cover. It was found that the free surface enters the drainpipe exactly at the same height as it was doing for an initial bath height of 20 mm. So it can be concluded that the initial bath height has no effect on the free surface as far as its arrival at the drainpipe is concerned.

With initial angular velocity. However, with the presence of an initial angular velocity the case is much different and interesting. When the drain cover is not present, the initial bath height influences the arrival of the free surface at the drainpipe when an initial angular velocity was imparted to the fluid. With the increase of the initial bath height, (h_i), the arrival of the free surface at the drainpipe (onset of air entrainment) was occurring at increased height of the free surface at the wall (h_a). Figure 7(a) shows the effect of initial bath height, h_i on h_a (the height of free surface at the wall) when the free surface arrives at the drainpipe with an initial angular velocity of 0.5 rad/s. It can be seen that h_a increases sharply with the increase of h_i. After a value of $h_i = 30$ mm, the increase of h_a becomes almost linear with h_i. Figure 7(b) shows the experimental snap shot when the free surface just enters the drainpipe. This experiment was conducted with an initial angular velocity of $\omega = 0.5\,\text{rad/s}$ with no drain cover having an initial height of water to be 125 mm in the vessel. From the experimental snap shot it can be seen that the height of the free surface at the vessel wall is 35 mm when air enters the drainpipe and the same can be read from Figure 7(a). Figure 7(a) shows a comparison of the height of the free surface at the vessel wall between the present computation and the experiment along with the volume of fluid drained. The comparison seems to be quite satisfactory except at lower initial bath height where some deviation from the experimental measurement can be seen, although the deviation is not too large.

When the drain cover is present the initial bath height does not influence h_a anymore. h_a remains constant even if the initial bath height increases along with the presence of a constant initial angular velocity.

Figure 8 shows the effect of initial bath height on the height of the free surface at the wall (h_a) when the free surface enters the drainpipe under a drain cover having an initial angular velocity of 1 rad/s. It can be seen that the initial bath height has no effect on the height of the free surface at the wall when the free surface enters the drainpipe. Figure 8(a) shows the free surface when the initial bath height was 20 mm and Figure 8(b) shows the case of an initial bath height of 40 mm. The shape and location of the free surface are almost identical, except very small near wall zone seen in Figure 8(b) where the height of the free surface is slightly lower compared to the case

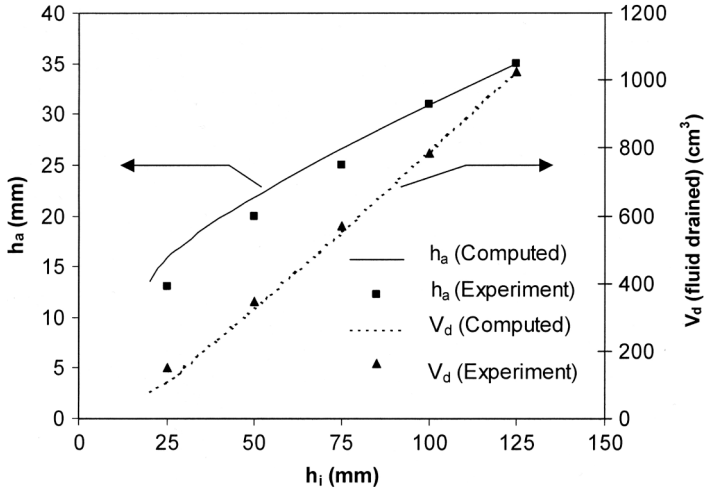

(a)

Effect of initial bath height of water on the height of the free surface at the wall and the amount of fluid drained when the free surface just enters the drainpipe, a comparison with experiment at $\omega = 0.5$ rad/s

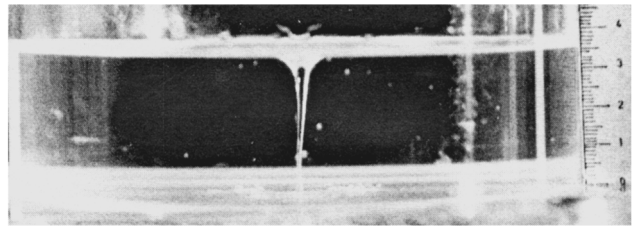

(b)

Experimental snap shot showing the free surface of water, when air just enters the drainpipe. Experiment conducted at initial $\omega = 0.5$ rad/s, with no drain cover, having an initial bath height of 125mm

Figure 7.

shown in Figure 8(a). The drain cover cuts down the effect of initial bath height and initial angular rotation on the arrival of the free surface at the drainpipe.

Conclusions

A numerical solution of the free surface of water in a cylindrical vessel has been made by using the finite volume approach with the incorporation of a VOF technique to predict the free surface. The effect of the drain cover, initial bath height and initial angular velocity has been studied on the arrival of the free surface at the inlet of the drainpipe. The following conclusions can be derived from the present numerical computation.

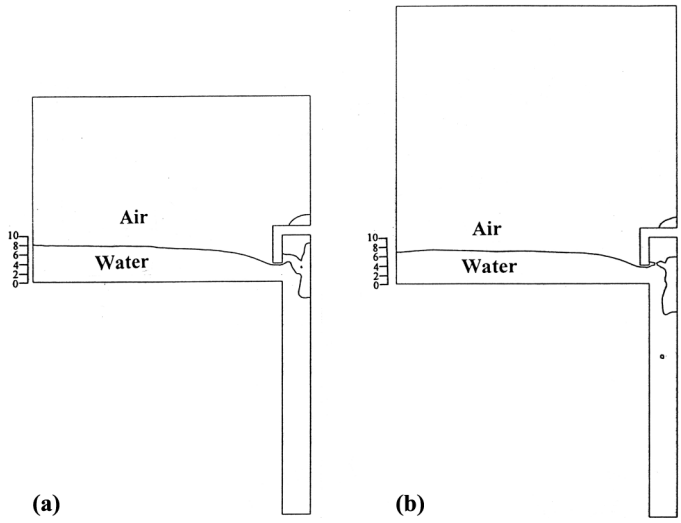

Figure 8.
Effect of initial bath height on the free surface of water entering the drainpipe having an initial angular velocity of 1.0 rad/s, initial bath height in: (a) 20 mm; (b) 40 mm, drain cover radius = 6 mm for both (a) and (b)

- An increase in the radius of the drain cover helps to drain more fluid without entrapping air into it.
- The presence of a drain cover eliminates the effect of initial bath height on the free surface of the liquid when it arrives at the drainpipe in the presence of an initial angular velocity.
- The presence of a drain cover cuts down the effect of initial disturbances on the formation of an air core and arrival of the free surface at the inlet of the drainpipe. The drain cover helps to delay the arrival of the free surface at the drainpipe, thereby causing more liquid to be drained without the entrapment of air.

Note

1. Comet User Manual, ICCM Institute of Computational Continuum Mechanics GmbH, Hamburg, Germany (www.iccm.de).

References

Baker, H.D. (1992), "Use of anti-vortexing devices in the tundish at LTV Steel Cleveland", *Steelmaking Conference Proceedings*, pp. 381-3.

Brackbill, J.U., Kothe, D.B. and Zemaach, C. (1992), "A continuum method for modeling surface tension", *Journal of Computer Physics*, Vol. 1, pp. 335-54.

Dash, S.K., Mondal, S.S. and Ajmani, S.K. (2004), "Mathematical simulation of surface wave created in a mold due to submerged entry nozzle", *International Journal of Numerical Methods for Heat & Fluid Flow*, Vol. 14 No. 5.

Dubke, M. and Schwerdtfeger, K. (1990), "Phenomena occurring during drainage of metallurgical vessels: effect of stopper rod on vortex formation and development of surface waves", *Ironmaking and Steelmaking*, Vol. 17 No. 3, pp. 184-92.

Hammerschmid, P., Tacke, K.H., Popper, H., Weber, L., Dubke, M. and Schwerdtfeger, K. (1984), "Vortex formation during drainage of metallurgical vessels", *Ironmaking and Steelmaking*, Vol. 11 No. 6.

Harleman, D.R.F., Morgan, R.I. and Purple, R.A. (1959), "Selective withdrawal from a vertically stratified fluid", International Association for Hydraulic Research, 8th Congress, Montreal, Paper 10C, pp. 1-16.

Muzaferija, S. and Peric, M. (1999), "Computation of free surface flow using interface-tracking and interface-capturing methods", in Mahrenholtz, O. and Markiewicz, M. (Eds), *Nonlinear Water Wave Interaction*, Chapter 2, WIT Press, Southampton, pp. 59-100.

Patankar, S.V. and Spalding, D.B. (1972), "A calculation procedure for heat, mass and momentum transfer in three-dimensional parabolic flows", *International Journal of Heat Mass Transfer*, Vol. 15, pp. 1787-806.

Steffen, R. (1987), "Fluid flow phenomena of metal and slag during drainage of metallurgical vessels", paper presented at the International Conference, Secondary Metallurgy, Editor Verein Deutscher Eisenhuttenleute (VDEh) Stahl Eisen.

Sankaranarayanan, R. and Guthrie, R.I.L. (1992), "A laboratory study of slag entrainment during the emptying of metallurgical vessels", *Steelmaking Conference Proceedings*, pp. 655-64.